DOI:10.31557/APJCC.2026.11.3.389

RESEARCH ARTICLE

Synthesis, and Evaluation of a 4,4′-Methylenedianiline-Based Ligand and some Complexes as Against Colorectal Cancer

Mohammed Kareem Ali[1]*, Haider Mohammed Hassoon[2]

[1]College of Science, Al-Qadisiyah University, Diwaniyah, Iraq. [2]Department of Chemistry, College of Science, Al-Qadisiyah University, Diwaniyah, Iraq.

Abstract

Introduction: The researchers sought to create a new bis-azo ligand as a progression of their previous studies. **Materials and Methods:** The ligand, designated as 6,6 (methylenebis (4,1-phenylene)) bis (diazene-2,1-diyl)) bis (2,4-dimethylphenol), was produced, followed by the preparation of a variety of chelate complexes with Pd^{+2}, and Au+3 ions. The characterization of these compounds was performed using advanced techniques such as elemental analysis, FT-IR spectroscopy, H, NMR spectroscopy, thermal analysis, through DSC to elucidate the synthesized complexes. **Results:** Analysis indicated that the complexes produced with Pd^{+2}, and Au^{+3} ions demonstrated a 2:1 metal-ligand ratio. The ligand was identified as bidentate (N-O) in nature. Molecular docking methods were employed to assess the effectiveness of these compounds in cancer treatment. The cytotoxicity of the 6-MPDDB dye ligand and its palladium (II) complex in colorectal carcinoma was assessed Using the MTT method. The dye and its metal complexes were evaluated for their antioxidant activity by assessing their ability to scavenge free radicals using the DPPH assay, with ascorbic acid serving as the standard. The IC_{50} values were determined, revealing that the ligand demonstrated notable free radical inhibition, whereas the antioxidant potential of the complexes differed according to their respective IC_{50} values. **Conclusion:** The synthesized ligand and its Pd(II) and Au(III) complexes demonstrated well-defined structural characteristics and promising biological activities. Overall, the results suggest their potential as effective antioxidant and anticancer agents, warranting further investigation.

Keywords: Bis-azo dye ligand- Bioactivity- anticancer- Spectroscopic studies- Molecular docking

Asian Pac J Cancer Care, **11 (3)**, 389-397 Submission Date: 01/06/2026 Acceptance Date: 03/07/2026

Introduction

Azo dyes currently predominate in global dye manufacturing chemistry, with their industrial significance anticipated to increase further in the future. They are essential in the administration of the dye and printing sector [1]. Synthetic and natural azo compounds serve as a crucial source of drug prototypes and a foundation for drug development, in addition to their use in other important applications. Moreover, due to their facile synthesis, elevated molar extinction coefficient, and superior wet fastness qualities, azo dyes hold significant importance of organic compounds [2, 3]. Mono-azo dyes represent the most prominent class of azo dyes [4], with a wide range of applications across diverse fields, including memory and recording devices [5, 6], molecular switches [7], thermochromic materials [8], catalysis [9], supramolecular systems [10], and textile and fiber dyeing. Their broad utility is largely attributed to their strong adsorption capacity and efficient interaction associated with the presence of the N=N group [11]. Azo ligands containing oxygen and nitrogen donor atoms are well known for their notable biological activity and excellent chelating ability toward various metal ions. Azo ligands can form coordination complexes with multiple metal ions, and the resulting properties of these complexes are highly dependent on the specific metal ion incorporated [12]. Azo ligand complexes possess diverse applications in medicine, including anticancer properties [9]. Antimicrobial, and anti-inflammatory agents [13]. Research on azo ligand complexes remains ongoing. These complex molecules possess numerous

Corresponding Author:
Dr. Mohammed Kareem Ali
Master's Degree, Department of Chemistry, College of Science, Al-Qadisiyah University, Diwaniyah, Iraq.
Email: mohammed.kareem@qu.edu.iq

potential applications, necessitating further investigation to fully understand their properties and prospective uses [9]. Their extensive applications arise from advantageous traits including synthetic flexibility, vibrant colors, and superior fastness characteristics. The azo compound is characterized by the nature of its substituents and their positions on the aromatic ring. The capacity of dyes to absorb electromagnetic energy within the visible spectrum (400-700 nm) dictates their coloration [14]. According to Witt's idea, a colored dye requires both an auxochrome and a chromophore group. Auxochromes enhance the color of a dye when included, while chromophores, including nitro, azo, and quinoid groups, impart color to the dye by absorbing visible light. The contemporary electronic theory has supplanted Witt theory. This concept posits that color arises from the excitation of valence p electrons by visible light (Murrell 1973) [15, 16]. Azo compounds possess a fundamental structure characterized by the azo functional group (-N=N-), which connects two organic substituents, including symmetric/asymmetric or symmetric/non-symmetric alkyl or aryl radicals [17]. The hues produced by azo dyes derive from the azo bonds and any associated chromophores or autochromes [18-20]. Numerous studies have demonstrated the effectiveness of light transition elements and heavy elements such as Au, Pd, and Pt when complexed with organic ligands as anti-cancer treatments [3, 21-23]. This study delineates the synthesis and characterisation of a novel bisazo dye ligand (6-MBTAMP) in conjunction with its complexes with Au (III), and Pd (II), metals, as well as its antibacterial, antifungal, antioxidant, and anticancer effects. Molecular docking was employed to assess the efficacy of these medicines in combating cancer. The cytotoxic effects of the ligand (6-MBTAMP) and its Pd (II) complex on colorectal cancer (CaCo2) were investigated. Subsequent study of the structure was conducted using elemental analysis (C.H.N), FT-IR, 1H-NMR, UV-Vis, XRD, and FE-SEM techniques.

Materials and Methods

All synthetic chemicals and solvents utilized in this study are of superior quality, sourced from reputable companies including BDH, Aldrich, Sigma, and Merck. 1H-NMR spectra were acquired using a Bruker BioSpin GmbH 400 MHz spectrophotometer, with DMSO-d6 as the solvent and TMS as the internal reference. The infrared spectra of all blend compounds were recorded using KBr pellets with a Bruker spectrophotometer (Germany) over the wavenumber range of 400-4000 -1cm. Essential examinations (C.H.N.S) were conducted utilizing a Euro (EA1106) elemental analyzer. The electronic spectra of the azo ligand and its metal complexes were recorded in a high ethanol solvent (10^-4 M) throughout the wavelength range of 1100 to 200 nm using a Shimadzu UV-650PC spectrophotometer (200-1100 nm) manufactured in Japan. At room temperature, attractive vulnerability assessments for pre-designed structures were conducted on an equilibrium attractive MSBMK utilizing the Faraday methodology. The Siemens model (D500) was utilized to calculate the X-ray beam refraction (XRD). Images of the ligand and its metal structures were obtained using a Field Emission Scanning Electron Microscope (FESEM) from the French Czech company T.E.S.C.A.N, namely the BRNOMira3 model.

Synthesis of 6,6 (methylenebis (4,1-phenylene)) bis (diazene-2,1-diyl)) bis (2,4-dimethylphenol) ligand (6-MBTAMP).

The synthesis of the 6-MBTAMP ligand was carried out as follows: 0.991 g (5 mmol) of 4,4′-methylenedianiline was dissolved in a mixture of 5 mL of 37% hydrochloric acid and 40 mL of distilled water. The resulting solution was cooled to a temperature between 0 and 5 °C. A separate solution containing 0.69 g (10 mmol) of sodium nitrite in 25 mL of distilled water was then added dropwise to the chilled mixture under continuous stirring, while ensuring the temperature remained below 5 °C throughout the addition. Independently, 1.222 g (10 mmol) of 2,4-dimethylphenol was solubilized in 17 mL of 10% NaOH and 30 mL of ethanol, then subjected to cooling. The previously prepared diazotized acid solution was gradually incorporated into this solution while stirring. This led to the creation of an insoluble orange liquid, which constituted the desired azo ligand. The precipitate was rinsed multiple times with a 1:1 solution of ethanol and water to eliminate inactive precursors. Ultimately, it was dried to yield the pure azo ligand. The reaction mechanism is delineated in Scheme 1. The multistep syntheses, which included diazotization and coupling processes, produced the necessary azo-containing ligand.

Preparation of [Pd (II), Au (III)] complexes

The metal complexes of the synthesized azo ligand were prepared using chloride salts of palladium (II), and gold (III). Each complex was formed in a 1:2 metal-to-ligand molar ratio, corresponding to the expected coordination geometry between the metal centers and the multidentate azo ligand. In a typical procedure, 0.177 g of $PdCl_2$, 0.394 g and of $HAuCl_4$ (each equivalent to 1 mmol) were gradually added dropwise to 15 mL of an ethanolic solution containing 0.232 g (0.5 mmol) of the ligand under continuous stirring. The reaction mixture was maintained at a temperature of 60–70°C for 3 hours to ensure complete complexion, then cooled in an ice bath to initiate precipitation. The mixture was allowed to stand overnight, after which the solid complexes were filtered,

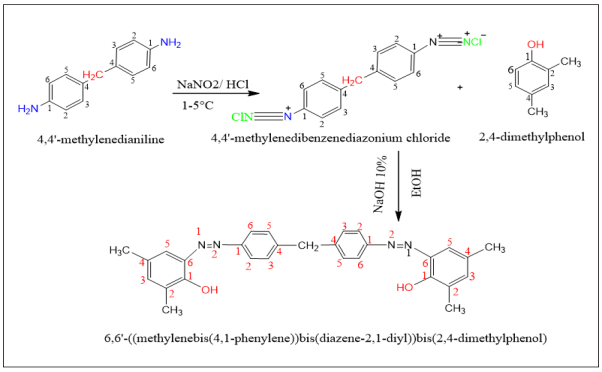

Scheme 1. Synthesis of ligand (6-MBTAMP)

Table 1. Analytical and Physical Properties of the Ligand and Its Complexes

o	Compound	M.wt g m/mole	Color	M.P(C°)	Yield	Elemental microanalysis%				
					(%)	C%	H%	N%	Cl%	M
1	$C_{29}H_{28}N_4O_2$	464.6	orange	178-180	73	74.98	6.08	12.06	-	-
						73.12	5.28	13.05		
2	$C_{32}H_{35}Au_2\ Cl_2N_4O_2$	1043.1	reddish orange	257-260	68	36.84	3.38	5.37	14.78	37.76
						35.21	2.39	5.11	13.59	38.2
3	$C_{30}H_{33}Cl_2N_4O_4Pd_2$	797.4	Dark brown	278-280	67	45.45	4.17	7.0 3	8.89	29.76
						44.16	3.24	6.82	9.88	30.22

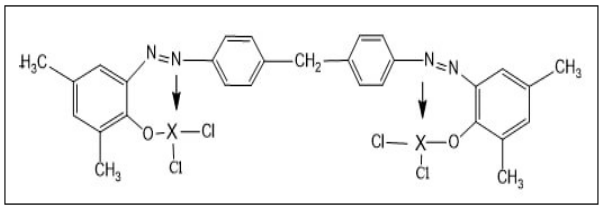

Scheme 2. Synthesis of Complexes where M Represents the Metals Au and Pd

washed thoroughly with distilled water followed by a small amount of hot ethanol to remove any unreacted materials, and finally dried in a vacuum desiccator. The gradual addition of reactants and precise stoichiometric control facilitated efficient coordination between the metal ions and the chelating azo ligand, yielding highly pure crystalline complexes. The analytical and physical characteristics of the ligand and its corresponding metal complexes are summarized in Table 1, and the synthetic route is illustrated in Scheme 2.

Results and Discussion

The synthesized azo ligand (6-MBTAMP) was obtained as a fine, amorphous orange powder. The amorphous character indicates the absence of a well-defined molecular arrangement, as evidenced by its varied solubility across different solvent systems. The ligand displayed high solubility in polar aprotic solvents such as dimethylformamide (DMF) and dimethyl sulfoxide (DMSO), which enabled precise spectroscopic characterization in solution. Ethanol was identified as the most effective solvent for recrystallization, yielding highly pure solid samples of 6-MBTAMP. The metal–ligand complexes formed from 6-MBTAMP exhibited pronounced stability under ambient conditions, and their analytical and physical characteristics, summarized in Table 1, showed excellent agreement with the theoretically predicted values.

1H-NMR spectra

The 1H-NMR spectra of the ligand, recorded in DMSO-d6 at 400 MHz, as depicted in Figure 1, exhibit signals indicative of the azo ligand. The 1H NMR spectrum displayed a wide singlet peak at δ (11.82) ppm (br s, 2H, Ar-OH), attributed to phenolic-OH protons. The chemical shift of aromatic protons on phenyl rings was attributed to the peaks at δ (7.03, 8.16) ppm, (m, 12H). The signal at 4.24 ppm was attributed to the protons of the benzylic CH2 (s, 2H, CH2 bridge). The methyl groups manifest as singlets at δ 2.41, 2.34, and 2.26 ppm (s, 12H, Ar-CH3), indicative of the lack of adjacent protons [24].

FT-IR spectroscopy

The ligand's infrared spectrum showed five distinct absorption bands at 3379, 3025, 2899, 1605, and 1511 cm^{-1}. These bands are linked to certain functional groups: The broad band at 3379 cm^{-1} is for the phenolic O–H stretch; the peaks at 3025 cm^{-1} and 2899 cm^{-1} are for the aromatic and aliphatic ν(C–H) vibrations of aryl-methyl substituents; the absorption at 1605 cm^{-1} is for the azo (–N=N–) group; and the band at 1511 cm^{-1} is for the aromatic ν (C=C) stretching within conjugated systems. A closer look at the IR spectra of all the metal complexes that were made showed that the phenolic O–H band had disappeared. This means that the hydroxyl group had lost its proton and was now coordinating with the metal ion. Moreover, the azo stretching band displayed significant shifts upon complexion, along with the emergence of new absorption indicative bands of M–N, M–O, and M–Cl vibrations. These changes in the spectrum show that the azo dye ligand binds to the metal center through two donor sites: the nitrogen atom in the azo group and the oxygen atom in the phenolic group. Hence, the ligand functions as an N,O-bidentate chelating agent in all synthesized metal complexes. Figure 2 shows the infrared spectrum of the prepared ligand [25, 26].

X-ray Diffraction

X-ray diffraction (XRD) analysis was conducted on the

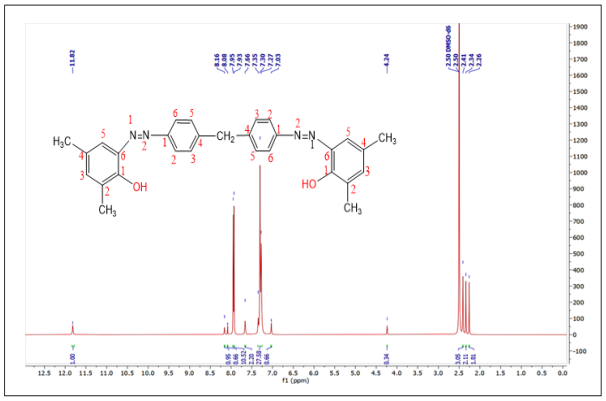

Figure 1. 1H-NMR Spectrum of Ligand (6-MBTAMP)

Table 2. Angles of Diffraction, d-observed Values, and Relative Intensities, Crystal Sizes, Crystal Tensions, Peak widths at Moderate Intensities, and Dissolution Densities for each of the Ligand and its Metal Complexes

Compound	Pos. [°2Th.]	Height [cts]	FWHM [°2Th.]	d-spacing [Å]	Rel. Int. [%]	Tip width [°2Th.]	Crystallite Size D (nm)	Dislocation density	Average size (nm)
6-MBTAMP	10.8464	122.52	0.4428	8.15034	16.61	0.5314	18.83	0.002820326	
	13.0214	358.93	0.492	6.79341	48.67	0.5904	16.98	0.003468364	25.85.
	15.3585	613.51	0.1968	5.76453	83.19	0.2362	42.56	0.000552073	
	15.6285	737.47	0.1968	5.66555	100	0.2362	42.57	0.000551814	
	16.4827	98.97	0.3936	5.37381	13.42	0.4723	21.31	0.002202	
	13.1691	10.57	0.5904	6.71759	22.63	0.7085	14.15	0.004994444	
6-MBTAMP Au	16.6831	46.69	0.2952	5.3097	100	0.3542	28.42	0.001238089	
	22.211	18.32	0.2952	3.99915	39.24	0.3542	28.66	0.00121744	25.89
	25.1276	9.12	0.2952	3.54117	19.53	0.3542	28.81	0.001204796	
	26.4517	15.95	0.3936	3.36684	34.16	0.4723	21.66	0.002131489	
	23.0613	106.78	0.1968	3.85357	21.55	0.2362	43.05	0.000539577	
6-MBTAMP Pd	27.9223	240.03	0.2952	3.19276	48.44	0.3542	28.97	0.001191525	27.92.
	29.4174	161.65	0.246	3.03381	32.63	0.2952	34.89	0.000821482	
	32.2989	494.67	0.246	2.76942	99.84	0.2952	35.13	0.000810296	
	32.7528	495.47	0.246	2.73208	100	0.2952	35.17	0.000808454	

samples using an X-ray diffractometer under controlled laboratory conditions. The resulting diffraction patterns displayed distinct peaks along the 2θ axis, representing the angles at which X-rays are deflected upon interacting with the sample. To extract quantitative data, the results were processed using specialized software, X'Pert HighScore, for detailed analysis.

The crystallite size was determined using the Scherrer equation, a well-established method for estimating particle size from XRD data. The analysis revealed that both the ligand (6-MBTAMP) and its metal complexes Au (III), Pd (II), and Ag (I) possess nanoscale dimensions, with the ligand exhibiting an average crystallite size of 25.85 nm, and the complexes showing average sizes of 27.92, 25.89, and 25.13 nm, respectively, as illustrated in Figure 3. These results confirm the nanostructured nature of the synthesized compounds, highlighting their potential applications in various technological and scientific fields that utilize the unique properties of nanomaterials.

Table 2 summarizes the structural parameters of the crystalline materials, including lattice strain, crystallite size, relative intensity, peak height, d-spacing, FWHM, peak position, and compound identification. These parameters provide insights into the crystallographic characteristics of the samples: lattice strain reflects internal stress, crystallite size indicates particle dimensions, and other values describe features such as peak intensity, interplanar spacing, and phase identification [27, 28].

Field-emission Scanning Electron Microscopy Analyzes For Bisazo Ligand (6MBD-DMP) and its metal complexes

Field-emission Scanning Electron Microscopy Analyzes For Bisazo Ligand (6MBD-DMP) and its metal complexes Field-emission scanning electron microscopy (FE-SEM) is a technique for examining the morphology, dimensions, and distribution of crystals, together with their crystalline and surface structures. Field-emission scanning electron microscopy was employed to capture images of the surfaces of ligand crystals and their metal complexes. This was due to its obvious demonstration of the disparities in crystal structures and surface homogeneity. It was utilized in the emission domain with a cross-sectional distance of 200 nm and a magnification factor of 50,000. The surface characteristics of Bisazo Ligand (6MPD-DDB) particles and their metal complexes were examined for particle size, morphology, aggregation, and distribution. The FE-SEM analysis image of the gold (III) complex revealed uneven, agglomerated crystals with an average particle size of 62.34nm. The FESEM images presented in Figure 4. indicate that the ligand and its metal complex under investigation possess a grain size of less than 100 nanometers, confirming its classification within the nanoscale range. This was corroborated by the XRD data and computations. The average crystal size (D) demonstrated relative consistency, hence affirming the validity of the data. Significantly, certain aggregates produced during the agglomeration process, which facilitates the assembly of elementary particles, pose challenges in eliminating this phenomenon due to the necessity of employing high temperatures to finalize the growth of ligand and complex crystals under preparation. The study therefore enhances the effective surface area,

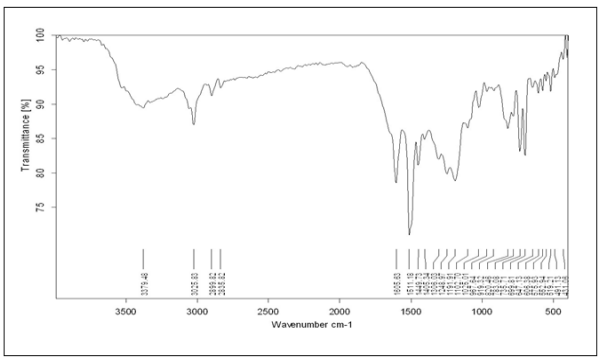

Figure 2. The IR Spectra of Ligand (6-MBTAMP)

Table 3. The Antioxidant Effects of the Ligand and its Pd (II) Complex

Compound %	inhibition				
	12.5 (µg/mL)	25 (µg/mL)	50 (µg/mL)	100 (µg/mL)	200 (µg/mL)
Ascorbic acid	30.71+1.0753	43.055+ 1.1040	53.973+1.2908	65.818+1.9516	76.389+1.4773
Complex	20.100+0.8533	24.884 +1.009	32.446 +3.1428	43.287+0.8737	51.311+2.0389

Table 4. The Impact of Pd Complex of CaCo-2 cells at 37°C Compared to a Control Cell Line at the Same Dose

Conc.(µg/ml)			HDFn	CaCo-2
Conc.	Mean	SD	Mean	SD
400	65.23933	2.315969	49.57567	2.974289
200	75.347	2.363498	66.281	1.279967
100	88.46433	0.707244	74.92267	0.928419
50	94.86867	0.267313	88.73467	1.871192
25	96.142	0.291464	94.25167	0.406382

which contributes to the quantitative effect, to generate new energy levels that facilitate electron movement. This characteristic inherent in the ligand and their synthesized metal complexes renders these compounds applicable in various domains. of biology and medicine as a treatment and the extent of the suitability of these compounds. In order to eliminate colorectal cancer (CaCo-2) [29, 30], and the possibility of using it or applying it as a medicine, will be explained later in our current study.

MTT test

The cytotoxic effects of CaCo-2, and HDFn were evaluated using Intron Biotech's ready-made MTT assay kit, which contained 1 mL of MTT solution in 10 vials, plus 50 mL of diluent in two vials. Tumor cells were cultured at concentrations ranging from 1×10^4 to 1×10^6 cells/mL in 96-well microplates, with a final volume of 200 µL of complete nutrient medium per well. The plates were then covered with sterile parafilm strips, gently agitated, and incubated at 37°C with 5% CO_2 for 72 hours. Following the incubation period, the medium was discarded, and bifold sequential concentrations of the compounds (400, 200, 100, 50, and 25 mg/mL) were added, with three replicates per concentration, in addition to controls containing cells treated with serum-free medium. The plates were then re-incubated under the same conditions for a 4-hour exposure. Subsequently, 20 µL of each compound was added to the wells and left to stand for 24 hours. Then, 10 µL of MTT solution was added to each well, and the incubation was repeated for an additional 4 hours. Finally, the medium was carefully discarded, and 100 µL of the solubilization solution was added to each well for 5 minutes. Absorbance was then measured using an ELISA reader at 575 nm. The absorption values were subjected to statistical analysis in order to calculate the required concentration of each compound to induce a 50% reduction in cell viability, using the equation:

$$Y = D + (A - D) / (1 + 10\text{^}(x - \log C)^B).$$

The anticancer activity of the synthesized palladium complex was evaluated against the human colorectal cancer cell line (CaCo-2) using the MTT assay. CaCo-2 cells were exposed to a series of concentrations of the complex (25, 50, 100, 200, and 400 µg/mL) to assess its effect on cell viability, as illustrated in Figure 8.

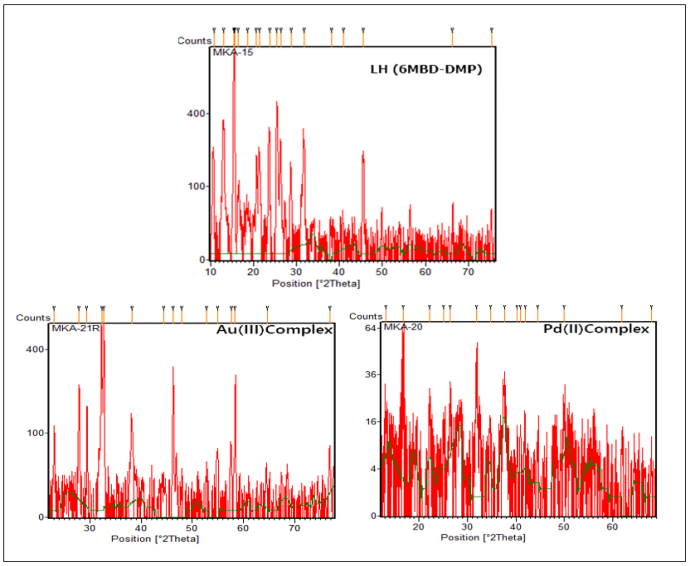

Figure 3. X-ray Diffraction Pattern of the Bis-azo Ligand ((6MBD-DMP)) and Its Complexes

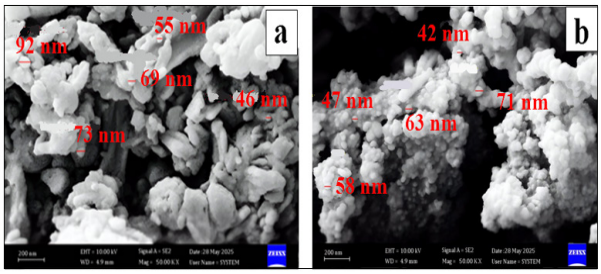

Figure 4. FESEM Images of the (a) Pd (b) Au Complexes

The reduction in CaCo-2 cell viability (%) after 72 hours of incubation with the palladium complex is summarized in Table 3 and Figure 8. The results demonstrated a concentration-dependent decrease in cell viability, with an IC_{50} value of 112.8 µg/mL. Significant cytotoxic effects were observed starting at 25 µg/mL, with a progressive increase in cell death up to 400 µg/mL ($P < 0.05$, $n = 6$). These findings indicate that the palladium complex exhibits a potent antiproliferative effect against CaCo-2 cells in a dose-dependent manner.

Additionally, notable morphological changes were observed in treated CaCo-2 cells. The pronounced cytotoxic activity of the complex may be attributed to its ability to induce apoptosis and cytotoxicity within cancer cells by reducing the proportion of cells in the G_0/G_1 and G_2/M phases of the cell cycle and by suppressing the mRNA expression of Bcl-2, an anti-apoptotic protein. This inhibition, in turn, promotes the activation of pro-apoptotic gene expression in cancer cells [31, 32]. Importantly, the palladium complex exhibited minimal cytotoxicity toward normal human dermal fibroblast neonatal (HDFn) cells, with an IC_{50} value exceeding 100 µg/mL, as shown in Figure 5, suggesting its selective toxicity toward cancerous cells (Table 4).

Microscopic analysis revealed a clear differential effect of the compound Pd complex on healthy fibroblasts (HDFn) compared to colon cancer cells (CaCo-2). HDFn cells retained their high density and characteristic normal morphology, with typical fibrous lines and elongation, and exhibited strong surface adhesion without any signs of cellular stress or apparent toxicity. This suggests that the compound exhibits low cytotoxicity towards healthy cells.

In contrast, CaCo-2 cells showed a marked decrease in number after treatment with the compound, and many appeared shrunken, spherical, or detached from the surface. Their morphological characteristics are generally associated with loss of viability and the initiation of cell death mechanisms such as apoptosis or necrosis. Large voids were also observed under the microscope, confirming the strong inhibitory effect of the compound Pd complex on cancer cell growth. Based on these results, the compound Pd complex exhibits high selectivity towards cancer cells, significantly inhibiting colon cancer cell growth with very limited effect on healthy cells. This selectivity highlights the importance of this compound as a promising candidate for anticancer therapeutic potential, while minimizing side effects on healthy tissues Figure 6 shows microscopic images of a Pd complex effect on healthy cells and treated cancer cells.

Antioxidant activity

The authors investigated the efficacy of the synthesized complex in scavenging free radicals by the stable DPPH free radical scavenging assay. DPPH is a stable radical due to the separation of the extra electron and the peak absorption at around 517 nm. Individuals frequently utilize DPPH's scavenging capability to assess the efficacy of various compounds in combating free radicals. Table 5 indicates that a concentration of 200 µg/mL of the complex exhibited the highest scavenging activity at 51.31 %. A higher concentration of the complex correlates with an increased percentage of free radicals it can scavenge. The synthesized complex has a similar free radical scavenging activity to that of the positive antioxidant ascorbic acid, particularly at concentrations between 50 and 100 g/mL (Figure 7). The concentrations of 200, 25, and 12.5 µg/ml showed the least action in comparison to ascorbic acid, which acted as a positive control. Pd complexes exhibit superior efficacy in scavenging DPPH compared to the associated free molecules [33, 34].

Molecular docking study

MOE is the new docking module (MOE, Vs. 2015) that is used to model how the tested drug interacts with functional cell proteins [35]. This simulation approach was applied to all synthesized ligands and complexes against the 2X6E protein. This study is an initial assessment designed to provide a comprehensive overview of the efficacy of the tested molecule (inhibitor) against the chosen pathogen. 2X6E shows how the Aurora-molecule looks in three dimensions. A kinase enzyme attached to a medication that stops colorectal cancer It is a protein enzyme that belongs to the serine/threonine kinase family. To begin, each molecule that was evaluated went through an energy minimization process to set up stable structures. Next, the MMFF94x force field adds atomic charges and

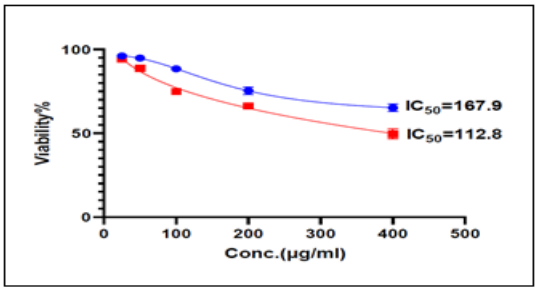

Figure 5. Cytotoxicity Effect of Pd Complex on Colorectal Cancer Cell Line.

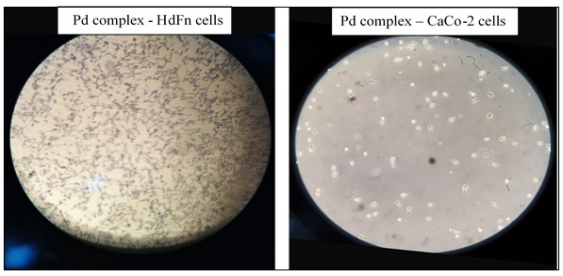

Figure 6. Microscopic Images of a Pd Complex Effect on HDFn Cells and CaCo-2 Cells.

Table 5. Docking Interaction Data for the Compounds, Ligand (6MBD-DMP), and Pd (Il) Complex for Ligand with the Active site of the Receptor of Colorectal Cancer. Aurora kinase A (AURKA) (PDB ID: 2X6E)

Compounds	S (kcal/mol)	RMSD	Ligand	Receptor	Interaction	Distance	E (kcal/mol)
Ligand	-7.01385784	2.35927749	6-ring	CG LEU 139 (A)	pi-H	3.81	-0.6
6MBD-DMP			6-ring	CA GLY 142 (A)	pi-H	4.35	-1.3
Pd (II) Mixed ligand	-7.31439209	1.95499635	PD 62	O LEU 139 (A)	metal	2.01	-2.2
			PD 63	OD1 ASP 274 (A)	metal	2.2	-5.4
			6-ring	CA GLY 140 (A)	pi-H	3.97	-0.8
			6-ring	CA GLY 216 (A)	pi-H	4	-0.6

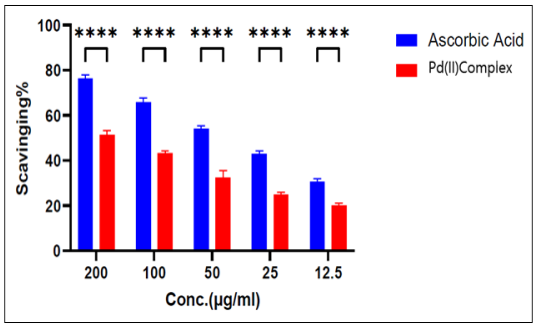

Figure 7. Antioxidant Activity of Pd (II) Complex Using DPPH

controls the potential energy and other settings. We put that chemical in a new database as an MDB file so that it could be utilized for docking experiments. Second, after removing the water molecules, hydrogen atoms were added to the amino acid receptors of each selected co-crystalline protein. Then, the potential energy was set, the site finder was controlled, and the domains over the alpha-site sphere were set [36]. So, the two sides are ready to simulate each process. The important interaction parameters were determined, and then the docking began till the process was finished. Using the London dG scoring algorithm, each process had an average of 30 poses. This was more than twice as good as the triangular Matcher approaches. In terms of extracted as ligand type, interaction type, receptors, bond length, and energy score value. The only Hbonding that works must be less than 3.5 Å. The docking validation patterns, surfaces, and maps were obtained following the ligand interaction process over line domains. To determine the ranking of inhibition efficiency, it is necessary to take into account the scoring energy, bond lengths, and receptors [37]. As presented in Table 5 and in Figure 8.

In conclusion, this study presents the synthesis and analysis of a novel ligand (6-MBTAMP) and its with three of its complexes: gold and palladium and silver. Theoretical data indicate that both complexes are square planar, while silver is tetrahedral, which is supported by magnetic and spectral evidence. The donor atoms coupled to the Au and Pd ion, with the ligand (6-MBTAMP) functioning as a bidentate ligand via coordinating through the nitrogen atom of the azo group and the oxygen atom of the carboxyl group. Molecular docking was employed to assess the activity of the metal complex against the colorectal cancer receptor protein, acquired from the (AURKA) protein data library. The oxidative status of the generated molecule was evaluated by assessing DPPH. The combined results indicated that the Pd (II)-complex had enhanced antioxidant activity relative to the free ligand (6-MBTAMP). Furthermore, the antitumoral efficacy against colorectal cancer cells (CaCo-2)

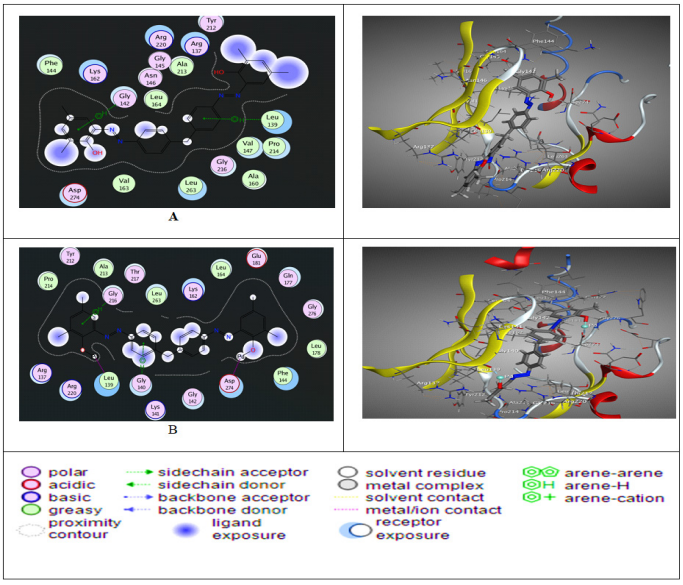

Figure 8. 2D and 3D Plot of the Interaction Between: (A) ligand (6MBD-DMP), and (B) Pd (II) Complex for Ligand with the Active site of the Receptor of Colorectal Cancer Aurora-A kinase (AURKA) (PDB ID: 2X6E) (D) Target Structure

demonstrated that the Pd (III) complex exhibited an IC50 of 112.8 µg/ml, indicating a more potent cytotoxic effect than the free ligand.

Acknowledgements

The authors express their sincere gratitude to the Department of Chemistry, College of Science, University of Al-Qadisiyah, for providing the necessary facilities and support to carry out this research work.

Statement of Transparency and Principles

• The authors declare no conflict of interest.

• The study was approved by the Research Ethics Committee of the authors' affiliated institution.

• The study data are available upon reasonable request.

Originality Declaration for Figures

All figures included in this manuscript are original and have been created by the authors specifically for the purposes of this study. No previously published or copyrighted images have been used. The authors confirm that all graphical elements, illustrations, and visual materials were generated from the data obtained in the course of this research or designed uniquely for this manuscript.

References

1. Mohammed HS, Al-Hasan HA, Chaieb Z, Zizi Z, Abed HN. Synthesis, characterization, DFT calculations and biological evaluation of azo dye ligand containing 1, 3-dimethylxanthine and its Co (II), Cu (II) and Zn (II) complexes. Bulletin of the Chemical Society of Ethiopia. 2023;37(2):347-56. https://doi.org/10.4314/bcse.v37i2.8
2. Eltaboni F, Bader N, El-Kailany R, Elsharif N, Ahmida A. Chemistry and Applications of Azo Dyes: A Comprehensive Review. Journal of Chemical Reviews. 2022 Oct 01;4(4):313-330. https://doi.org/10.22034/jcr.2022.349827.1177
3. Sahar YJ, Mohammed H, Al-Abady ZN. Synthesis and characterization of new metal complexes containing azo-indole moiety and anti-leukemia human (HL-60) study of its palladium (II) complex. Results in Chemistry. 2023;5:100847. https://doi.org/10.1016/j.rechem.2023.100847
4. Rashidnejad H, Ramezanitaghartapeh M, Pesyan NN, Mahon PJ, Raposo MMM, Coelho PJ, Lup ANK, Soltani A. A comprehensive spectroscopic, solvatochromic and photochemical analysis of 5-hydroxyquinoline and 8-hydroxyquinoline mono-azo dyes. Journal of Molecular Structure. 2021 01 05;1223:129323. https://doi.org/10.1016/j.molstruc.2020.129323
5. Park H, Kim E-R, Kim DJ, Lee H. Synthesis of metal-azo dyes and their optical and thermal properties as recording materials for DVD-R. Bulletin of the Chemical Society of Japan. 2002;75(9):2067-70. https://doi.org/10.1246/bcsj.75.2067
6. Gao T, Xue Y, Zhang Z, Que W. Multi-wavelength optical data processing and recording based on azo-dyes doped organic-inorganic hybrid film. Optics Express. 2018 02 19;26(4):4309-4317. https://doi.org/10.1364/OE.26.004309
7. Anger E, Fletcher SP. Simple azo dyes provide access to versatile chiroptical switches. European Journal of Organic Chemistry. 2015;2015(17):3651-5. https://doi.org/10.1002/ejoc.201500485
8. Soreño ZV, Puguan JMC, Kim H. Thermochromic transition analysis of elastomer prepared from azo dye-siloxane blend. Materials Chemistry and Physics. 2020;240:122297. https://doi.org/10.1016/j.matchemphys.2019.122297
9. El-Ghamry HA, Alharbi BK, Takroni KM, Khedr AM. A series of nanosized Cu (II) complexes based on sulfonamide azo dye ligands: an insight into complexes molecular structures, antimicrobial, antitumor and catalytic performance for oxidative dimerization of 2-aminophenol. Applied Organometallic Chemistry. 2023;37(2):e6978.https://doi.org/10.1002/aoc.6978
10. Ferreira GR, Marcial BL, Garcia HC, Faulstich FR, Dos Santos HF, de Oliveira LFC. Supramolecular compounds of azo dyes derived from 1-phenylazo-2-naphthol and their nickel and copper complexes. Supramolecular Chemistry. 2015;27(1-2):13-20.
11. Omar AZ, El-Rahman MA, El-Sadany SK, Hamed EA, El-Atawy MA. Synthesis of novel bisazo disperse dyes: Spectroscopic characterization, DFT study and dyeing of polyester. Dyes and Pigments. 2021 Dec 01;196:109831. https://doi.org/10.1016/j.dyepig.2021.109831
12. Almáši M, Vilková M, Bednarčík J. Synthesis, characterization and spectral properties of novel azo-azomethine-tetracarboxylic Schiff base ligand and its Co(II), Ni(II), Cu(II) and Pd(II) complexes. Inorganica Chimica Acta. 2021 01 24;515:120064. https://doi.org/10.1016/j.ica.2020.120064
13. Abd El-Lateef HM, Khalaf MM, Gouda M, Amer AA, Abdelhamid AA, Abdou A. Design, synthesis of new mixed azo-hydroxyquinoline complexes; in vitro anti-inflammatory, antifungal, antibacterial, theoretical, and molecular docking interactions Investigation. Journal of Molecular Structure. 2024;1307:138016. https://doi.org/10.1016/j.molstruc.2024.138016
14. Ibraheem IH, Mubder NS, Abdullah MM, Al-Neshmi H. Synthesis, characterization and bioactivity Study from azo – ligand derived frommethyl-2-amino benzoatewith some metal ions. Baghdad Science Journal. 2023 02 01;20(1). https://doi.org/10.21123/bsj.2022.6584
15. Reda SM, Al-Hamdani AAS. Mn (II), Fe (III), Co (II) and Rh (III) complexes with azo ligand: Synthesis, characterization, thermal analysis and bioactivity. Baghdad Science Journal. 2023;20(3):0642. https://doi.org/10.21123/bsj.2022.7289
16. Dhamra M. Spectrophotometric determination of tranexamic acid by azo-dye formation-application to pharmaceutical preparations. Journal of Education and Science. 2011;24(3):21.0-33.0. https://doi.org/10.33899/edusj.1999.58803
17. Kyhoiesh HAK, Al-Adilee KJ. Synthesis, spectral characterization, antimicrobial evaluation studies and cytotoxic activity of some transition metal complexes with tridentate (N,N,O) donor azo dye ligand. Results in Chemistry. 2021 01 01;3:100245. https://doi.org/10.1016/j.rechem.2021.100245
18. Nagasundaram N, Govindhan C, Sumitha S, Sedhu N, Raguvaran K, Santhosh S, et al. Synthesis, characterization and biological evaluation of novel azo fused 2, 3-dihydro-1H-perimidine derivatives: In vitro antibacterial, antibiofilm, anti-quorum sensing, DFT, in silico ADME and Molecular docking studies. Journal of Molecular Structure. 2022;1248:131437. https://doi.org/10.1016/j.molstruc.2021.131437
19. El-Habeeb AA, Refat MS. Synthesis, structure interpretation, antimicrobial and anticancer studies of tranexamic acid

complexes towards Ga (III), W (VI), Y (III) and Si (IV) metal ions. Journal of Molecular Structure. 2019;1175:65-72. https://doi.org/10.1016/j.molstruc.2018.07.099
20. Keshavayya J, Pushpavathi I, Keerthikumar CT, Maliyappa MR, Ravi BN. Synthesis, characterization, computational and biological studies of nitrothiazole incorporated heterocyclic azo dyes. Structural Chemistry. 2020 08 01;31(4):1317-1329. https://doi.org/10.1007/s11224-020-01493-0
21. Lashanizadegan M, Ashari HA, Sarkheil M, Anafcheh M, Jahangiry S. New Cu (II), Co (II) and Ni (II) azo-Schiff base complexes: Synthesis, characterization, catalytic oxidation of alkenes and DFT study. Polyhedron. 2021;200:115148. https://doi.org/10.1016/j.poly.2021.115148
22. Kazim NH, Khadim LH. Study of Suggested Chemotherapy Agent of bis ((S) -3-methoxycarbamoyl pentanoate) di chloride bis (ethyl amine) platinum (IV))MPP) using DFT. Egyptian Journal of Chemistry. 2021 07 01;64(7):3405-3411. https://doi.org/10.21608/ejchem.2021.62383.3338
23. Kazim NH, Khadim LH. Molecular Modeling Study to Propose a New Model of Cisplatin (IV) Complex as chemotherapy for cancer. Journal of Kufa for Chemical Sciences. 2021;2(7):152-164.
24. Hamza IS, Al-Daffaay RKH, Faris SS, Al-Hamdani AAS. Ru+3, Rh+3, Pd+2,Pt+4 and Au+3 Metal ions Complexes with Azo Derived from 4-Aminomethyl-cyclohexane carboxylic acid Synthesis, Characterization, Thermal Study and Antioxidant Activity. Iraqi Journal of Science. 2025 03 30;1010-1024. https://doi.org/10.24996/ijs.2025.66.3.3
25. Hamza IS, Mahmmoud WA, Al-Hamdani AA, Ahmed SD, Allaf AW, Al Zoubi W. Synthesis, characterization, and bioactivity of several metal complexes of (4-Amino-N-(5-methyl-isaxazol-3-yl)-benzenesulfonamide). Inorganic Chemistry Communications. 2022 Oct 01;144:109776. https://doi.org/10.1016/j.inoche.2022.109776
26. Hadi MA, Kareem IK. synthesis, Characterization and Spectral Studies of a new Azo-Schiff base Ligand Derived from 3, 4-diamino benzophenone and its Complexes with Selected Metal Ions. Research Journal in Advanced Sciences. 2020;1(1):54-73.
27. Mohammed MK, Mohammad M, Jabir M, Ahmed D, editors. Functionalization, characterization, and antibacterial activity of single wall and multi wall carbon nanotubes. IOP Conference Series: Materials Science and Engineering; 2020: IOP Publishing.
28. Khashan K, Jabir M, Abdulameer F, editors. Preparation and characterization of copper oxide nanoparticles decorated carbon nanoparticles using laser ablation in liquid. Journal of Physics: Conference Series; 2018: IOP Publishing.
29. Shieh Y, Liu G, Wu H, Lee C. Effects of polarity and pH on the solubility of acid-treated carbon nanotubes in different media. Carbon. 2007 08 01;45:1880-1890. https://doi.org/10.1016/j.carbon.2007.04.028
30. Lim EWC, Feng R. Agglomeration of magnetic nanoparticles. The Journal of Chemical Physics. 2012 03 28;136(12):124109. https://doi.org/10.1063/1.3697865
31. Mohammed AH, Muthanna FMS, Hassan BAR, Karuppannan M, Wayyes AM. Impact and Association of Anaemia Severity and Its Treatment With Quality of Life of Breast Cancer Patients in Malaysia. Iraqi Journal of Pharmaceutical Sciences. 2022 Dec 23;31(2):62-70. https://doi.org/10.31351/vol31iss2pp62-70
32. alladeen M. Study the effect of drying methods On the quality characteristics for dill and parsley. Muthanna Journal for Agricultural Sciences. 2023 Dec 15;10:1-20. https://doi.org/10.52113/mjas04/10.2/24
33. Sadowska-Bartosz I, Bartosz G. Antioxidant Activity of Anthocyanins and Anthocyanidins: A Critical Review. International Journal of Molecular Sciences. 2024 Nov 08;25(22):12001. https://doi.org/10.3390/ijms252212001
34. Tumilaar SG, Hardianto A, Dohi H, Kurnia D. A Comprehensive Review of Free Radicals, Oxidative Stress, and Antioxidants: Overview, Clinical Applications, Global Perspectives, Future Directions, and Mechanisms of Antioxidant Activity of Flavonoid Compounds. Journal of Chemistry. 2024;2024(1):5594386. https://doi.org/10.1155/2024/5594386
35. Mashat K, Babgi B, Hussien PM, Arshad MN, Abdellattif M. Synthesis, structures, DNA-binding and anticancer activities of some copper(I)-phosphine complexes. Polyhedron. 2019 01 15;158:164-172. https://doi.org/10.1016/j.poly.2018.10.062
36. Abdellattif M, Hussien PM, Alzahrani E. New Approaches Of 4-Aryl-2-Hydrazinothiazole Derivatives Synthesis, Molecular Docking, And Biological Evaluations. International Journal of Pharmaceutical Sciences. 2018 01 01;9:1000-1019. https://doi.org/10.13040/IJPSR.0975-8232.9(12).5060-78
37. El-Metwaly N, Farghaly T, Elghalban M. Synthesis, analytical and spectral characterization for new VO (II)-triazole complexes; conformational study beside MOE docking simulation features. Applied Organometallic Chemistry. 2020 01 18;34. https://doi.org/10.1002/aoc.5505